Full Paper

Journal of the Brazilian Chemical Society

https://dx.doi.org/10.21577/0103-5053.20260008

J. Braz. Chem. Soc. **2026**, *37-Spe1*, e-20260008, 1-14

Reanalysis of Public Metabolomics Data Reveals Class-Specific Dysregulation of *N*-Acyl Lipids and Related Molecules in Atopic Dermatitis

Natâna S. Cunha,[a,b] *Anthony R. Moreira,*[a,c] *Tainara C. Vieira,*[a,d] *Sandro D. Souza,*[a,e] *José Diogo E. Reis*[a,b] *and Paulo Wender P. Gomes*[*,a,b,c,e]

[a]*Central Integrada em Metabolômica da Amazônia, Instituto de Ciências Exatas e Naturais, Universidade Federal do Pará, 66075-110 Belém-PA, Brazil*

[b]*Programa de Pós-Graduação em Química, Instituto de Ciências Exatas e Naturais, Universidade Federal do Pará, 66075-110 Belém-PA, Brazil*

[c]*Faculdade de Química, Instituto de Ciências Exatas e Naturais, Universidade Federal do Pará, 66075-110 Belém-PA, Brazil*

[d]*Faculdade de Farmácia, Instituto de Ciências da Saúde, Universidade Federal do Pará, 66075-110 Belém-PA, Brazil*

[e]*Programa de Pós-Graduação em Biodiversidade e Biotecnologia (BIONORTE), Universidade Federal do Pará, 66075-110 Belém-PA, Brazil*

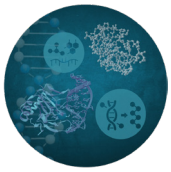

Atopic dermatitis (AD) is a chronic inflammatory skin condition marked by impaired epidermal barrier function and substantial alterations in lipid homeostasis. While previous metabolomics studies have characterized major lipid classes involved in skin physiology, the contribution of *N*-acyl lipids and related molecules to AD remains poorly defined. In this study, an integrative reanalysis of the public mass spectrometry interactive virtual environment (MassIVE) dataset is performed combining fold-change statistics, global natural product social molecular networking (GNPS), and fast mass spectrometry search tool (fastMASST). Among the 6,332 mass spectrometry (MS) features detected, 12 were annotated. These compounds were assigned as putative identifications (level 2), based on tandem mass spectrometry (MS/MS) spectral similarity, molecular networking relationships, and *in silico* fragmentation analysis. Though, their identities were not confirmed with authentic reference standards. The annotated compounds belong to three chemically distinct subclasses: (*i*) *N*-acylethanolamines and long-chain amides, (*ii*) carnitines, and (*iii*) *N*-acyl amino acids, dipeptides, and related derivatives. These subclasses exhibited distinct class-specific behavior, characterized by increased levels in AD lesion samples. fastMASST searches further indicated that several of these molecules are widely co-occurring in microbial and personal-care product datasets, providing potential microbiome- and exposome-context for their presence in skin affected by atopic dermatitis. Together, these findings reveal a distinct class-specific signature of *N*-acyl lipid, carnitines, and amino acids/dipeptides that are associated with the dysregulation in AD, and thereby, demonstrating the power of public data reanalysis to uncover previously overlooked biochemical patterns associated with skin barrier dysfunction.

Keywords: atopic dermatitis, skin barrier, *N*-acyl lipids, metabolomics, exposomics, GNPS

Introduction

Atopic dermatitis (AD) is a highly prevalent chronic inflammatory skin disorder that affects up to 20% of children and 10% of adults worldwide, imposing a substantial burden on quality of life and healthcare systems. It is characterized by intense itching, recurrent inflammation, and loss of epidermal barrier integrity.[1] The barrier dysfunction in AD arises from both structural abnormalities in the stratum corneum and altered lipid composition, particularly involving ceramides, fatty acids, and acylated signaling lipids.[2] These lipid classes are essential for maintaining epidermal cohesion, hydration, antimicrobial defense, and immune homeostasis, and their dysregulation is a central feature of AD pathophysiology.[3]

*e-mail: wendergomes@ufpa.br
Editor handled this article: Hector Henrique F. Koolen (Associate)
This publication is part of the special issue "Omics Sciences".

Classical epidermal lipids, including ceramides, cholesterol, and free fatty acids, have been extensively studied in the context of AD. Reduced ceramide content, altered fatty acid chain length, and disrupted lipid organization are well-established contributors to impaired barrier function, increased transepidermal water loss, and enhanced susceptibility to inflammation and microbial colonization.[3,4] However, these well-characterized lipid classes do not fully explain the biochemical complexity of lipid dysregulation observed in atopic skin, suggesting that additional, less-studied lipid mediators may also play important roles.

Among lipid classes, *N*-acyl lipids-including *N*-acyl ethanolamines, *N*-acyl amino acids, and related amides-play crucial roles in cutaneous homeostasis and inflammation control.[4] They act through pathways involving endocannabinoid receptors (CB1/CB2), peroxisome proliferator-activated receptors (PPARs), and lipid remodeling enzymes such as *N*-acyltransferases and fatty acid amide hydrolases (FAAHs).[5,6] Despite their established biological activity and relevance to inflammatory signaling, *N*-acyl lipids have received far less attention in AD research than classical epidermal lipids, and their specific contribution to barrier integrity and inflammatory processes in AD remains largely uncharacterized. This knowledge gap represents an unmet need in understanding the full lipidomic landscape of atopic dermatitis.

To address this gap, an analytical strategy capable of comprehensively capturing chemically diverse and structurally related *N*-acyl lipid species is required. Public metabolomics data re-mining, particularly when combined with a curated *N*-acyl lipid MS/MS library,[7] provides a powerful and targeted solution. In many untargeted metabolomics studies, *N*-acyl lipids are detected but not explicitly annotated or interpreted, as they were not the primary focus of the original investigation. Reanalysis of public liquid chromatography tandem mass spectrometry (LC-MS/MS) datasets therefore enables systematic exploration of these overlooked lipid subclasses without the need for new sample collection, while promoting data reuse and analytical transparency.

Metabolomics, particularly untargeted LC-MS/MS, enables the large-scale detection and annotation of small molecules in biological systems.[8] A single LC-MS/MS run can yield thousands of tandem mass spectrometry (MS/MS) spectra, and public repositories such as mass spectrometry interactive virtual environment (MassIVE) provide access to millions of such spectra. These resources support data re-mining approaches, in which advances in computational tools allow new biological insights to be extracted from existing datasets.[9] Key bioinformatic strategies include molecular networking on GNPS, which enables the organization of MS/MS spectra based on structural similarity and supports chemical class annotation across studies. This can be combined with fold-change calculations[10,11] to prioritize metabolites showing biologically meaningful differences between conditions. Mass spectrometry search tool (MASST) searches[12] further extend this framework by contextualizing molecular features across diverse biological and environmental datasets, including plants,[13] microbes,[14] foods,[15] drugs,[16] thereby enhancing interpretation while remaining exploratory in nature.

In this study, we explicitly aimed to comprehensively characterize class-specific alterations of *N*-acyl lipids and related molecules in atopic dermatitis skin through integrative reanalysis of publicly available LC-MS/MS data. Leveraging a public skin metabolomics dataset, we performed a systematic re-mining workflow centered on GNPS molecular networking, fold-change-based statistical filtering, and MASST contextualization. This approach revealed a previously underexplored dysregulation of *N*-acyl lipids organized into three structurally distinct subclasses. Based on this framework, targeted re-mining of public LC-MS/MS data would uncover *N*-acyl lipid signatures and related molecules associated with AD that were not captured in the original analysis. Because this study is based on observational public data, the identified associations are exploratory and hypothesis-generating. Nevertheless, the class-specific patterns reported here provide a new biochemical perspective on lipid imbalance in AD and demonstrate the value of public metabolomics data reanalysis for uncovering overlooked molecular features relevant to skin barrier dysfunction.

Methodology

Dataset retrieval and pre-processing

This study is based on the reanalysis of a publicly available LC-MS/MS dataset (MassIVE accession: MSV000090788)[17] originally generated to compare healthy skin and atopic dermatitis lesion samples. The original study included 30 healthy controls and 30 AD lesion samples, representing biological replicates (Ethics Committee 2021-100691-BO-ff). All samples were acquired using the same LC-MS/MS platform, comprising a Vanquish UHPLC system coupled to a Q-Exactive Orbitrap mass spectrometer (Thermo Fisher Scientific, Germany), and detailed methods on sample preparation and chromatography are described in the previous publication.[18] The generated data were then processed using MZmine v4.8.30 (mzio GmbH, Bremen, Germany, 2025),[19] applying the following settings: MS^1

and MS^2 mass detection were performed using minimum intensity thresholds of 1.0×10^5 and 1.0×10^3, respectively. Chromatograms were constructed using the ADAP chromatogram builder, with a minimum group size of three scans, a minimum group intensity of 1.0×10^5, a maximum group intensity of 3.0×10^5, and an *m/z* tolerance of 0.002 Da. Savitzky-Golay smoothing was applied using a window of five scans, followed by chromatographic deconvolution using the local minimum feature resolver. Deconvolution parameters included a chromatographic threshold of 90%, a minimum peak separation of 0.05 min, a minimum absolute peak height of 1.0×10^5, a peak area coefficient of 1.70, a peak duration ranging from 0.05 to 1.0 min, and a minimum of three data points *per* peak. Isotope detection was performed using the isotope peak grouper with *m/z* and retention time tolerances of 10 ppm and 0.2 min, respectively, assuming charge state 1 for the most intense isotope. Feature alignment and duplicate removal were conducted using the same *m/z* and retention time tolerances, with weighting factors of 75% for *m/z* and 25% for retention time. Metacorrelation grouping and ion identity networking were subsequently applied to identify peak correlations and adduct relationships. The resulting peak lists (exported as .MGF and .CSV files) were filtered to remove features derived from blanks (≥ 300% intensity relative to samples), followed by normalization and missing-value imputation using feature-based molecular networking (FBMN) stats.[20] The final filtered dataset consisted of 6,332 features, which served as the input for all subsequent statistical analyses.

Fold-change calculation and statistical filtering

Differential analysis was performed using the MS feature intensity table retrieved from the MZmine data re-processing step. All data processing and statistical calculations were conducted in the the R environment (version 2024.09.1, R Foundation for Statistical Computing, Austria, 2024). Before analysis, feature intensities were preprocessed to handle zero values. For each feature, a minimum positive intensity value was identified across both sample groups. Zero values were then imputed with a value equivalent to one-tenth of this minimum to approximate the limit of detection and enable logarithmic transformation. The processed raw data consisted of 6,332 MS features across 30 healthy control and 30 AD lesion samples.

For each MS feature, the following were calculated: (*i*) the percentage of samples in which the feature was detected (non-zero intensity) within each group; (*ii*) the mean intensity (avg_healthy, avg_ADlesion) and the mean log10-transformed intensity (avg_log_healthy, avg_log_ADlesion) for each group. FC values were calculated in both directions (healthy/AD and AD/healthy) using both raw and log-transformed mean intensities. A non-parametric Wilcoxon rank-sum test was applied to compare the intensity distributions between healthy and AD groups, generating a *p*-value for each feature. The resulting *p*-values were adjusted for multiple hypothesis testing using the Benjamini-Hochberg method to control the false discovery rate (FDR), yielding an adjusted *p*-value. Features with an absolute fold-change (AD/healthy) greater than 2.0 and an adjusted FDR *p*-value of less than 0.05 were considered statistically significant. A fold-change threshold of 2.0 was selected as a conservative and commonly used cutoff in untargeted metabolomics to prioritize metabolites showing biologically meaningful differences while limiting the influence of technical variability, particularly in reanalyzes of public datasets where experimental conditions cannot be controlled. For data visualization, scatter plots were generated in a Jupyter Notebook environment using pandas (v7.3.2, NumFOCUS, USA, 2025) Python-based (v3.10, Python Software Foundation, USA, 2025). Data handling and preprocessing were performed using pandas (v3.0.0, NumFOCUS,USA, 2025), developed by Wes McKinney. Interactive visualizations were created using plotly.express, part of the Plotly library (v6.5.0, Plotly Technologies Inc., Canada, USA, 2025). These MS features were also selected for further library searching integrated to feature-based molecular networking on the GNPS platform.[21]

Molecular networking and annotation of *N*-acyl lipids

The significant MS features identified through statistical filtering were analyzed using the FBMN workflow on the GNPS2 platform.[22] The results are publicly accessible.[23] The parameters were set as follows: mass tolerances for precursor and fragment ions were 0.02 Da, a minimum cosine score of 0.7, and 4 matched peaks were required for spectral similarity, the maximum number of neighbors *per* node was 10, and the maximum number of molecular families was 100.

To specifically target the chemical class of interest, all spectra within the network were searched against a new library of *N*-acyl lipids and related molecules[7] in addition to the experimental and propagated GNPS spectral libraries.[21] For library matching, a cosine score of 0.6 and a minimum of 4 matched fragment ions were applied. The resulting molecular network was downloaded and visualized using Cytoscape software (version 3.10.3, Cytoscape Consortium, NRNB, USA, 2024)[24] to explore the structural relationships and annotate the dysregulated *N*-acyl lipid or structurally related molecules.

Classification of *N*-acyl lipid and related molecules

Annotated compounds through the GNPS *N*-acyl lipids library were categorized into three structural subclasses: (*i*) *N*-acylethanolamines and long-chain amides (amide-linked fatty acids to ethanolamine or amine backbones); (*ii*) carnitines; and (*iii*) *N*-acyl amino acids and dipeptides (amide or ester conjugates of amino acids). To further validate this classification, MS/MS spectra from .mgf file for all annotated molecules were processed using SIRIUS 6.0.[25] This *in silico* tool was used to compute molecular fingerprints and classify the compounds based on their structural fingerprints and fragmentation tree ranking, providing orthogonal confirmation of the proposed subclasses.

fastMASST searches for biological and exposome context

To investigate the potential clinical, microbial, and environmental sources of the annotated molecules, a batch MASST[12] analysis was performed using the Python MASST batch via command line.[26] The universal spectrum identifiers (USIs) of the filtered and annotated *N*-acyl lipids and or related molecules were compiled into an input file (Table S1, Supplementary Information (SI) section). This file was submitted to the fast search API (Application Programming Interface) to query multiple domain-specific databases simultaneously. The search parameters were set to a minimum cosine score of 0.7, a fragment ion *m/z* tolerance of 0.02 Da, a precursor ion *m/z* tolerance of 0.02 Da, and required a minimum of 3 matched fragment ions. The search was executed against the metabolomics repository. The output files for different domains were filtered to determine the prevalence and sources of the annotated *N*-acyl lipids across microbial taxa and personal care products.

fastMASST data visualization

The MASST[12] search results for microbial and personal care product datasets were integrated and visualized using UpSet plots[27] to illustrate the co-occurrence of the annotated *N*-acyl compounds across different sources for these molecules. The data matrices, detailing the presence of each compound within specific microbial genera and personal care categories, were processed using a custom Python script. The plots were configured to sort both the individual sets and their intersections by cardinality, which efficiently displays the complex set relationships.

Results

Class-specific dysregulation of *N*-acyl lipids and derivatives in atopic dermatitis

Our reanalysis pipeline, which combined GNPS molecular networking, fold-change statistics, and MS/MS-based annotation, as illustrated in Figure 1a, enabled the annotation of a pronounced dysregulation of *N*-acyl lipids and related molecules in skin affected by AD lesion. Among the 6,332 MS features detected across all raw LC-MS/MS files, statistical comparison of AD lesions to healthy skin (fold-change AD/healthy ≥ 2.0 and FDR-adjusted $p \leq 0.05$) identified 102 significantly dysregulated metabolites (Figure 1b). Although features enriched in healthy skin were also detected (Figure 1b), the present analysis and subsequent annotation were intentionally restricted to metabolites showing increased relative abundance in AD lesion samples, with a focus on *N*-acyl lipids and related molecules. Subsequent annotation efforts established that 12 of these discriminant MS features belonged to the broad chemical class of *N*-acyl lipids/carnitines and amino acid-derived conjugates. To structurally characterize these discriminant features, we performed manual curation of MS/MS spectra integrated with feature-based molecular networking on the GNPS platform. This approach, combining spectral library matching and substructure-based annotation propagation, enabled high-confidence Level-2 annotation according to the Metabolomics Standards Initiative (MSI)[28] for 12 of the significant features. Strikingly, all annotated compounds belonged to the broad chemical category of *N*-acyl lipids and structural derivatives.

The SIRIUS[25] classification was reflected in the molecular networking topology, where each subclass formed at least one independent, non-overlapping cluster within the GNPS molecular network (Figure 1c), revealed that these 12 metabolites consistently segregated into three chemically and biosynthetically distinct subclasses based on their structural backbones (Figure 1d): (*i*) *N*-acylethanolamines and long-chain amides (1-3); (*ii*) carnitines (4), and (*iii*) *N*-acyl amino acids and dipeptides (5-8). Intriguingly, these clusters contained numerous other connected molecules; these other derivatives were not present with significant fold-changes in the AD samples, suggesting a highly specific dysregulation. Also, the absence of spectral connections between these three molecular families indicates a lack of shared major fragmentation pathways, reinforcing the hypothesis that these metabolite classes originate from distinct biosynthetic routes and are subject to separate catabolic processes. Together, these findings reveal a coordinated yet class-specific dysregulation of

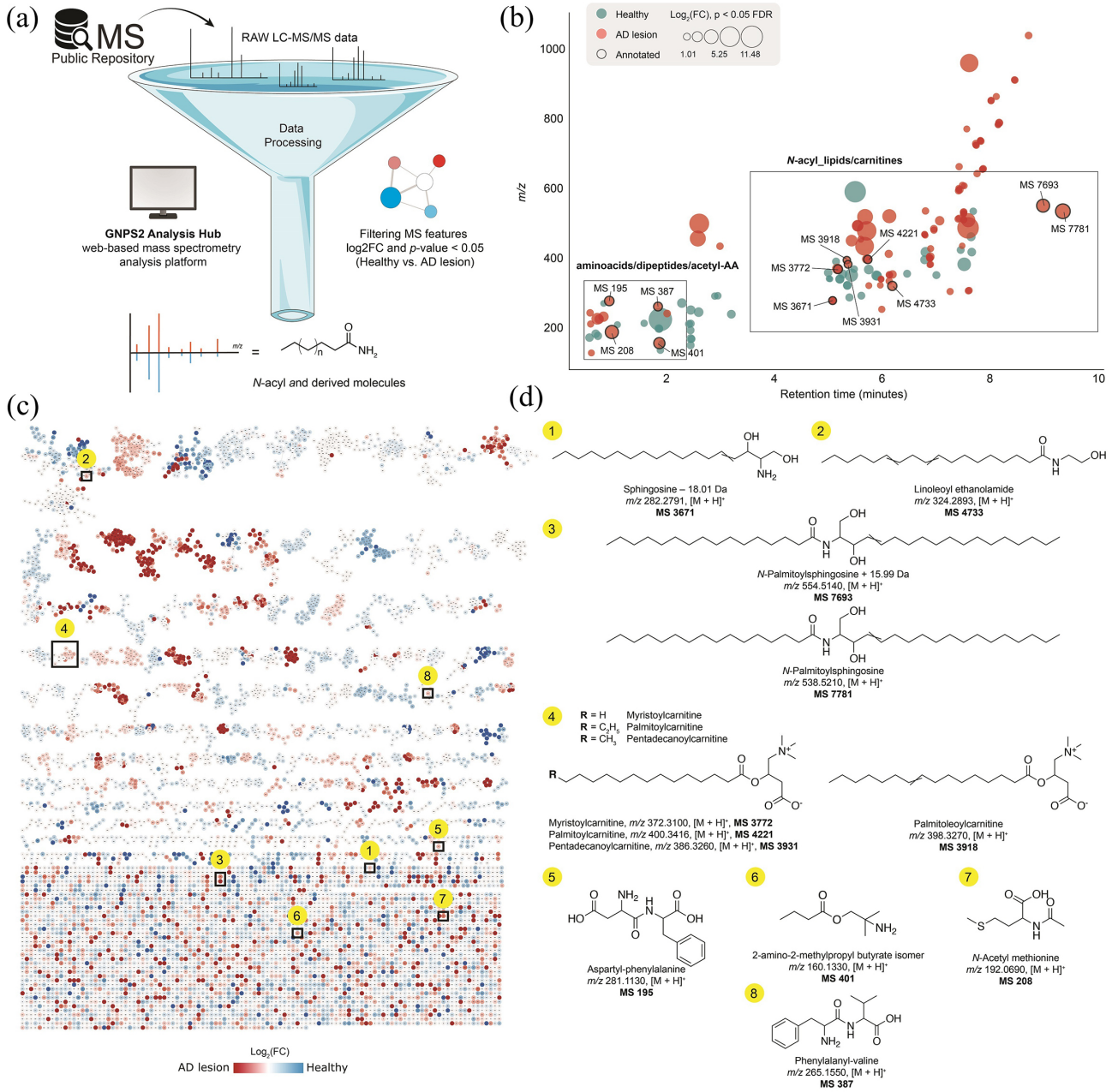

Figure 1. Reanalysis of public skin metabolomics data reveals class-specific dysregulation of *N*-acyl lipids and related molecules in AD. (a) Workflow for reanalysis of public LC-MS/MS dataset from MassIVE, integrated to GNPS2 molecular networking, and statistical filtering (FC ≥ 2.0, FDR ≤ 0.05) to map discriminatory features between healthy skin and AD lesion skin; (b) filtered MS features plotted as *m/z versus* retention time, colored by enrichment based on Log2 fold-change (red: AD lesion; blue: healthy). Bubble size reflects fold-change magnitude, and red boxes indicate AD lesion samples enriched in *N*-acyl lipids/carnitines and amino acids/dipeptides. Enrichment indicates higher relative abundance, not exclusive detection; (c) GNPS molecular networking of *N*-acyl lipids and related molecular families, with nodes colored by differential abundance (red: AD lesion; blue: healthy). Clustering reflects spectral similarity; (d) twelve (12) annotated metabolites (MSI level 2) with enrichment patterns in AD lesion samples.

the *N*-acylated metabolome, pointing to a multifaceted disruption of lipid signaling and barrier composition in atopic skin.

Compound assignment

The first subclass of *N*-acyl lipids, *N*-palmitoylsphingosine (*m/z* 538.5210), exhibited a remarkably diagnostic MS/MS spectrum that exemplifies characteristics of *N*-acyl ethanolamines and long-chain acylamides. As shown in Figure 2a, the precursor ion undergoes an initial neutral loss of a $C_{16}H_{30}O$ moiety, corresponding to the cleavage of the palmitoyl chain from the sphingoid base backbone. This transformation generates the protonated long-chain amino alcohol fragment at *m/z* 282.28, which serves as the central branching point for subsequent diagnostic

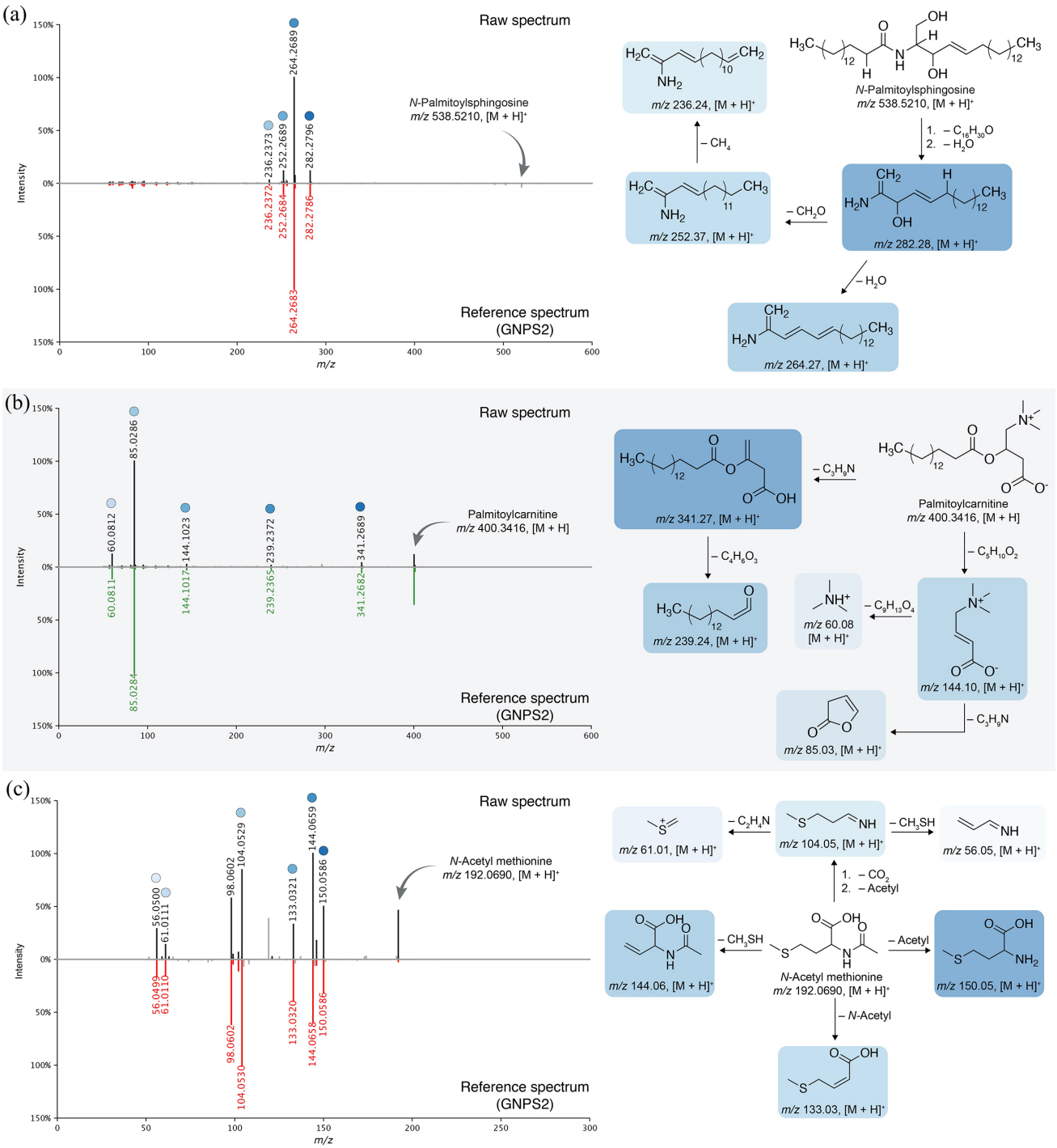

Figure 2. Representative MS/MS fragmentation profiles for key metabolites from the three annotated *N*-acyl subclasses. Panel (a) highlights chain-specific cleavages of *N*-palmitoylsphingosine; panel (b) highlights chain-specific cleavages of palmitoylcarnitine; and panel (c) shows characteristic neutral losses and sulfur-based fragments of *N*-acetyl methionine. Together, these spectra illustrate the conserved diagnostic patterns supporting these subclass annotations.

reactions. This fragment retains the unsaturated sphingoid chain and the amino alcohol moiety, giving rise to two canonical low-mass products: (*i*) H_2O loss, producing the dehydrated ion at *m/z* 264.27, consistent with β-elimination reactions of protonated amino alcohols;[29] and (*ii*) loss of CH_2O, yielding the ion at *m/z* 252.37, reflecting cleavage at the C_1–OH region of the sphingoid backbone.[30] A further loss of CH_4 from the *m/z* 252.37 intermediate produces the characteristic low-mass reporter ion at *m/z* 236.24, a diagnostic signature in sphingoid-base fragmentation pathways. The clean, sequential neutral losses and chain-specific cleavage signatures collectively reinforce the conserved fragmentation architecture typical of long-chain *N*-acylated amino alcohols within this subclass.

Other members of this molecular family, such as two sphingosine-derived (*m/z* 554.5140, and 282.2791) and linoleoyl ethanolamide (*m/z* 324.2893), exhibited comparable fragmentation logic, and their corresponding GNPS mirror plots are provided in Figures S1-S3 (SI section). Note that the observed +15.99 Da mass shift of *m/z* 554.5140 corresponds to an oxidized analog of *N*-palmitoylsphingosine, most likely reflecting hydroxylation, and was annotated using an analog suspect library[31] containing millions of *in silico* MS/MS spectra to support annotation propagation.

The second subclass of *N*-acyl derived is exemplified by palmitoylcarnitine (*m/z* 400.3416, $[M + H]^+$), which shows a highly diagnostic MS/MS spectrum (Figure 2b) dominated by two complementary dissociation routes that separately report on the acyl chain and the carnitine headgroup. As shown in Figure 2b, the precursor ion of *m/z* 400.3416 first undergoes a characteristic neutral loss of C_3H_4N, generating the product ion at *m/z* 341.27 ($[M + H]^+$). We hypothesize this fragment acts as a central intermediate for subsequent chain-associated cleavage, and it further dissociates via loss of $C_4H_6O_3$ to yield the prominent ion at *m/z* 239.24 ($[M + H]^+$), consistent with a stabilized long-chain acyl-derived fragment that is commonly observed for fatty-acyl esters.[32] In parallel, palmitoylcarnitine produces a second diagnostic branch centered on the carnitine moiety. The precursor ion also fragments via loss of $C_5H_{10}O_2$, producing the headgroup-rich ion at *m/z* 144.10 ($[M + H]^+$). This fragment then serves as a branching point for two canonical low-mass reporter ions: (*i*) loss of C_3H_4N to generate *m/z* 85.03 ($[M + H]^+$); and (*ii*) loss of $C_9H_{13}O_4$ to generate the highly characteristic ion at *m/z* 60.08 ($[M + H]^+$). The combination of these sequential neutral losses yields a consistent fragmentation logic for the acyl-chain and carnitine-derived pathway, also observed in the other three acyl carnitines (Figures S4-S6, SI section).

Last, the third subclass of amino acids and dipeptides includes *N*-acetyl methionine (*m/z* 192.0690), 2-amino-2-methylpropyl butyrate isomer (*m/z* 160.1330), aspartyl-phenylalanine (*m/z* 281.1130), and phenylalanyl-valine (*m/z* 265.1550). Among these, *N*-acetyl methionine displayed a rich MS/MS spectrum, making it an ideal representative example to illustrate the characteristic features of this molecular subclass fragmentation profile. As shown in Figure 2c, its spectrum exhibits prominent fragment ions at *m/z* 150.05, 144.06, 133.03, 104.05, 61.01, and 56.05, corresponding to sequential neutral losses and side-chain cleavages fully consistent with *N*-acylated methionine fragmentation.[33] These include (*i*) loss of the *N*-acetyl group (*m/z* 150.05), (*ii*) neutral loss of methanothiol (*m/z* 144.06), (*iii*) *N*-acetyl loss followed by insaturation (*m/z* 133.03), and (*iv*) combined decarboxylation and deacetylation at *m/z* 104.05, followed by the series of sulfur-based fragment ions at *m/z* 61.01 and 56.05. The remaining metabolites of this subclass showed similarly clean and predictable MS/MS patterns dominated by neutral losses typical of amino acid conjugates (e.g., CO_2, NH_3),[33] as illustrated in the GNPS mirror plots provided in Figures S7-S9 (SI section). Together, these features offered strong structural confidence, placing these compounds into a coherent and chemically related molecular family.

MASST-based source of *N*-acyl-based molecules

microbeMASST searching

To investigate the potential microbial origin or modification of the dysregulated *N*-acyl lipids and related compounds, we performed a MASST similarity search against public microbial metabolomics datasets, including bacteria, fungi, and environmental microbiota. MicrobeMASST analysis revealed that the annotated *N*-acyl lipids are widely distributed across diverse microbial sources. As shown in the UpSet plot (Figure 3a), the bacterial datasets exhibit substantial compound-dependent variability in detection frequency and taxonomic distribution. Among the annotated metabolites, phenylalanyl-valine displays the highest overall set size and the largest single intersection, indicating that this dipeptide is widely and consistently detected across diverse bacterial genera. This broad occurrence contrasts with several *N*-acyl lipids, such as palmitoylcarnitine and myristoylcarnitine, which appear in fewer datasets and intersections.

In contrast, *N*-palmitoylsphingosine and its oxidized analog (+15.99 Da) show extensive taxonomic breadth, with matches spanning numerous bacterial genera across multiple intersections, highlighting their widespread - but more heterogeneous - distribution. These include anaerobic gut-associated taxa (e.g., *Bacteroides*, *Parabacteroides*, *Prevotella*), and Gram-positive genera (e.g., *Streptomyces*, *Staphylococcus*, *Bacillus*, *Enterococcus*). This consistent co-occurrence across all compounds emphasizes the metabolic versatility of this dominant anaerobic gut genus. It raises the possibility that some of the *N*-acyl lipid and related molecules observed in human skin may arise from or be modulated by the microbial metabolic activity.

On the other hand, as shown in Figure 3b, the microbeMASST search against fungal datasets yielded a smaller number of matches and fewer intersections compared to the bacterial datasets. Four metabolites - phenylalanyl-

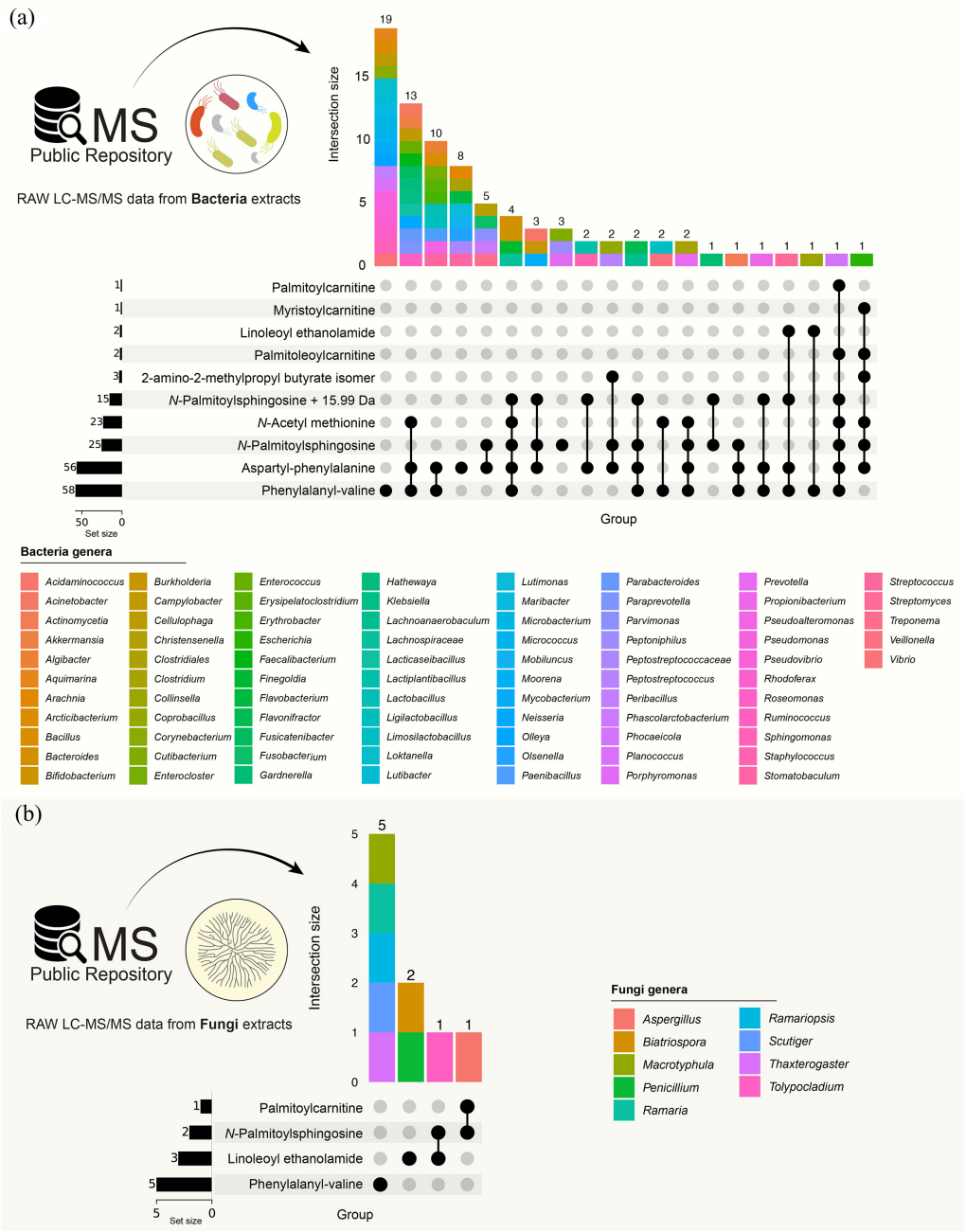

Figure 3. MicrobeMASST analysis shows that the dysregulated *N*-acyl lipids and related compounds annotated in this study are broadly distributed across microbial metabolomics datasets. The intersection plot highlights compounds that are frequently detected across multiple (a) Gram-negative and Gram-positive bacteria; (b) fungi datasets. The genus-level summary shows that these detections span a broad taxonomic range.

valine, linoleoyl ethanolamide, *N*-palmitoylsphingosine, and palmitoylcarnitine - were detected across a limited number of fungal taxa, including *Penicillium*, *aspergillus*, *Ramaria*, *Macrotyphula*, *Scutiger*, *Thaxterogaster*, *Biatriospora*, and *Tolypocladium*. Phenylalanyl-valine exhibited the largest set size among the fungal-associated metabolites, while the remaining compounds were detected in one to three datasets. At the genus level, these matches indicate that most detections were compound-specific, with few shared occurrences across multiple fungal genera.

Personal care MASST searching

Some AD-related molecules could be coming from personal care products. To evaluate this, we queried all annotated molecules against publicly available LC-MS/MS datasets derived from personal care products. As shown in Figure 4, three metabolites - linoleoyl ethanolamide, aspartyl-phenylalanine, and phenylalanyl-valine - were detected across personal care product datasets. Among these, linoleoyl ethanolamide exhibited the largest set size,

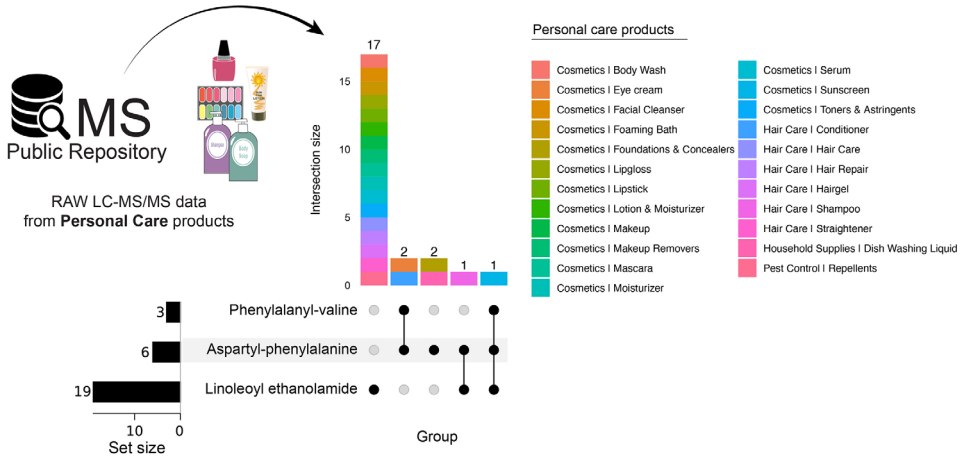

Figure 4. Personal care MASST analysis showing the occurrence of dysregulated metabolites in consumer product LC-MS/MS datasets. The UpSet intersection plot highlights the detection frequency and co-occurrence patterns of linoleoyl ethanolamide, aspartyl-phenylalanine, and phenylalanyl-valine across personal care product datasets.

appearing in 19 datasets, followed by aspartyl-phenylalanine detected in 6 datasets, and phenylalanyl-valine detected in 3 datasets. The intersection analysis shows that most detections correspond to linoleoyl ethanolamide alone, with the largest single intersection comprising 17 datasets, while smaller intersections reflect co-occurrence with one or both dipeptides. At the product-category level, detections spanned a range of personal care formulations, including cosmetics (e.g., body wash, facial cleansers, moisturizers, makeup and makeup removers, lip products, toners, serums, sunscreens), hair care products (e.g., shampoos, conditioners, hair repair and styling products), as well as household and pest-control related products.

Discussion

The primary objective of this study was to perform a class-specific reanalysis of publicly available LC-MS/MS skin metabolomics data to investigate the contribution of *N*-acyl lipids to atopic dermatitis. The observations described in this section are directly supported by relative abundance patterns derived from LC-MS/MS data, whereas subsequent biological interpretations are intended to be hypothesis-generating and association-based. Using an integrative workflow combining molecular networking, fold-change-based filtering, and MS/MS-guided annotation, we identified a coherent and reproducible dysregulation of *N*-acyl lipids and related molecules between healthy skin (n = 30) and AD lesion samples (n = 30). *Post hoc* power analysis based on observed effect sizes indicated that most discriminatory features were sufficiently powered (α = 0.05, power = 0.80) with the available sample size (n = 30 *per* group), supporting the robustness of the reported associations.

By integrating fold-change statistics, molecular networking, and MS/MS-based annotation, we filtered and annotated three structurally distinct subclasses, specifically *N*-acyl lipids, carnitines, and amino acids/dipeptides, which were predominantly enriched in AD lesion samples. The observed alterations were consistent across multiple molecular features within each subclass and across most samples, rather than being driven by a small subset of individual metabolites or outlier samples, as reflected by coherent fold-change patterns and molecular networking structure. Previous studies[34-36] also support the consistency of these lipid-associated patterns across multiple molecular features. These observations are consistent with the notion that an imbalance of *N*-acyl lipids and related molecules may represent a biochemical feature of the atopic epidermis. The higher relative abundance of these subclasses in AD lesions, together with their lower relative abundance in healthy skin, reflects enrichment in disease samples rather than condition-exclusive detection. Given the known involvement of these molecules in epidermal homeostasis through pathways such as PPAR-α activation, endocannabinoid signaling, and ceramide metabolism,[37,38] these class-level shifts may be relevant to barrier dysfunction in AD, although such interpretations remain hypothesis-generating.

Moreover, the accumulation of *N*-acyl lipids and related molecules in AD lesions is consistent with altered downstream metabolic turnover,[39] potentially involving pathways associated with amidases, peptidases, or conjugate hydrolases, although such enzymatic changes cannot be directly inferred from the present LC-MS/MS data. These molecules have been reported in prior studies to participate in processes such as pH buffering, microbial interactions, and keratinocyte communication,

and their increased relative abundance may reflect a compensatory metabolic response to barrier stress.[40] The tight clustering of these features within molecular networks indicates shared MS/MS fragmentation patterns and coordinated class-level behavior, rather than confirmed pathway-level regulation. Taken together, the class-specific patterns observed are consistent with a multifaceted alteration of *N*-acyl lipid remodeling, potentially involving both enzymatic and non-enzymatic (e.g., oxidative) influences.[41] Such alterations may be associated with weakened lipid organization, reduced anti-inflammatory lipid tone, and increased susceptibility to environmental or microbial stressors,[42,43] although these interpretations remain hypothesis-generating. Overall, the findings support an association between *N*-acyl lipid dysregulation and barrier dysfunction in AD,[44] based on metabolic associations derived from LC-MS/MS data, and are intended to be hypothesis-generating rather than mechanistic conclusions.

MASST matches were used to contextualize the environmental, microbial, or consumer-product-associated detection space of related MS/MS features, rather than to infer biological origin or function, which revealed compound-dependent microbial occurrence patterns for the dysregulated *N*-acyl lipids[45] and related molecules (Figure 3). Several metabolites, particularly phenylalanyl-valine, were detected across a broad range of bacterial genera, whereas others, such as palmitoylcarnitine and linoleoyl ethanolamide, showed more restricted distributions. Given the well-documented dysbiosis in AD,[46] shifts in microbial community structure may influence the abundance or turnover of amino acid conjugates. In this context, the oxidized analog of *N*-palmitoylsphingosine was detected across multiple bacterial genera, while detections in fungal datasets were comparatively limited. Together, these observations indicate that a subset of the dysregulated metabolites in AD skin have microbial analogs or are associated with microbial metabolic space. Although MASST co-occurrence indicates spectral similarity across datasets and provides contextual information on where related molecules have been previously detected, it does not demonstrate biological origin, direct transfer, or functional activity in atopic skin.

Exposome analysis provided additional context for interpreting these metabolic signatures. No direct microbiological profiling or environmental exposure measurements were performed in this study. Microbiome- and exposome-related interpretations are therefore speculative and presented as hypothesis-generating contextual frameworks. Personal care MASST searching (Figure 4) showed that linoleoyl ethanolamide, aspartyl-phenylalanine, and phenylalanyl-valine were detected across publicly available LC-MS/MS datasets derived from consumer products, including cosmetics, hair care formulations, and household-related products. Linoleoyl ethanolamide showed the highest detection frequency, while the dipeptides were observed in fewer datasets. These findings indicate that a subset of metabolites enriched in atopic skin may also be potentially present in consumer formulations, which is particularly relevant in the context of a compromised epidermal barrier. Such product-associated compounds may supplement, mimic, or interfere with endogenous *N*-acyl lipid signaling, potentially contributing to the observed metabolic alterations.[47]

These combined observations support a model in which dysregulated *N*-acyl lipid and related molecules metabolism reflects the intersection of endogenous enzymatic imbalance,[44] oxidative stress,[48,49] microbial remodeling,[50] and environmental exposures.[51] The loss of protective long-chain amides weakens barrier lipid homeostasis, while the accumulation of amino acid conjugates suggests stalled turnover or compensatory metabolic activation.[52,53] The appearance of oxidized lipid analogs indicates chemical stress resulting from lipid oxidation or co-metabolism between microbes and the host. Together, these processes converge to reshape the *N*-acyl lipid landscape, potentially contributing to the structural and immunological abnormalities characteristic of atopic dermatitis.[54] Despite these insights, this study has limitations inherent to the reanalysis of publicly available metabolomics data. First, the findings are derived from a single observational LC-MS/MS dataset and were not supported by targeted experimental validation or replication in an independent patient cohort. Although the original study included a balanced design with 30 healthy and 30 atopic dermatitis samples, and *post hoc* power analysis indicates that most discriminatory features were sufficiently powered, the absence of external validation limits the generalizability of the reported associations. Moreover, observational metabolomics data do not allow causal inference regarding biological function, metabolic origin, or disease mechanisms. Accordingly, the class-specific dysregulation of *N*-acyl lipids and related molecules reported here should be interpreted as exploratory and hypothesis-generating. Future studies involving larger and independent cohorts, as well as targeted and functional validation approaches, will be essential to confirm the robustness, reproducibility, and biological relevance of these associations.

Conclusions

N-Acyl lipids and related molecules are a prominent and class-specifically dysregulated component of the

metabolic landscape associated with atopic dermatitis. The distinct alterations observed across *N*-acyl amino acids and dipeptides, *N*-acylethanolamines and long-chain amides, and carnitine-conjugated fatty acids are consistent with perturbations in acylation balance, amide turnover, and oxidative lipid remodeling, processes that are essential for maintaining epidermal structure and chemical defense. By leveraging large-scale public LC-MS/MS datasets, this work highlights previously underexplored dimensions of *N*-acyl lipid metabolism and places these alterations within a broader chemical context that includes microbial metabolic space and consumer product-associated exposures. While MASST-based analyses do not establish causality, they provide valuable insight into the potential ecological and exposomic relevance of the dysregulated metabolites observed in atopic skin. Together, these findings position *N*-acyl lipid and related molecule homeostasis as a promising source of candidate biomarkers and mechanistic targets, offering a framework for future targeted studies aimed at understanding barrier dysfunction and inflammatory regulation in atopic dermatitis.

Supplementary Information

Supplementary information (Table S1 and Figures S1-S9) is available free of charge at http://jbcs.sbq.org.br as PDF file.

Data Availability Statement

The dataset with all LC-MS/MS files is publicly available in the MassIVE repository [Link] under the accession number MSV000090788.[17] Code used for data analysis is available at [Link].

Acknowledgments

N.S.C. and all co-authors are thankful to the CIMAZON from the UFPA for providing computational infrastructure for the dataset reanalysis and CNPq (443823/2024-3 - Call CNPq/MCTI/FNDCT No. 19/2024 PRO AMAZONIA).

Author Contributions

Conceptualization, methodology, formal analysis, data curation, investigation, visualization, writing original draft: NSC. Conceptualization, supervision, funding acquisition, project administration, writing (review and editing): PWPG. Methodology, data curation, formal analysis, writing (review and editing): ARM. Data curation, software, methodology: TCV. Investigation, data curation, validation: SDS. Formal analysis, validation, visualization, writing (review and editing): JDER. All authors have read and agreed to the published version of the manuscript.

References

1. Weidinger, S.; Beck, L. A.; Bieber, T.; Kabashima, K.; Irvine, A. D.; *Nat. Rev. Dis. Primers* **2018**, *4*, 1. [Crossref]
2. Lee, A.-Y.; *Int. J. Mol. Sci.* **2020**, *21*, 1194. [Crossref]
3. Kim, B. E.; Leung, D. Y. M.; *Allergy Asthma Immunol. Res.* **2018**, *10*, 207. [Crossref]
4. Nicolaou, A.; Kendall, A. C.; *Pharmacol. Ther.* **2024**, *260*, 108681. [Crossref]
5. Maccarrone, M.; Di Marzo, V.; Gertsch, J.; Grether, U.; Howlett, A. C.; Hua, T.; Makriyannis, A.; Piomelli, D.; Ueda, N.; van der Stelt, M.; *Pharmacol. Rev.* **2023**, *75*, 885. [Crossref]
6. Uyama, T.; Sasaki, S.; Okada-Iwabu, M.; Murakami, M.; *Int. J. Mol. Sci.* **2025**, *26*, 3359. [Crossref]
7. Mannochio-Russo, H.; Charron-Lamoureux, V.; van Faassen, M.; Lamichhane, S.; Gonçalves Nunes, W. D.; Deleray, V.; Ayala, A. V.; Tanaka, Y.; Patan, A.; Vittali, K.; Rajkumar, P.; El Abiead, Y.; Zhao, H. N.; Gomes, P. W. P.; Mohanty, I.; Lee, C.; Sund, A.; Sharma, M.; Liu, Y.; Pattynama, D.; Walker, G. T.; Norton, G. J.; Khatib, L.; Andalibi, M. S.; Wang, C. X.; Ellis, R. J.; Moore, D. J.; Iudicello, J. E.; Franklin, D. , Jr; Letendre, S.; Chin, L.; Walker, C.; Renwick, S.; Zemlin, J.; Meehan, M. J.; Song, X.; Kasper, D.; Burcham, Z.; Kim, J. J.; Kadakia, S.; Raffatellu, M.; Bode, L.; Chu, H.; Zengler, K.; Wang, M.; Siegel, D.; Knight, R.; Dorrestein, P. C.; *Cell* **2025**, *188*, 4154. [Crossref]
8. Clish, C. B.; *Cold Spring Harbor Mol. Case Stud.* **2015**, *1*, a000588. [Crossref]
9. El Abiead, Y.; Strobel, M.; Payne, T.; Fahy, E.; O'Donovan, C.; Subramamiam, S.; Vizcaíno, J. A.; Yurekten, O.; Deleray, V.; Zuffa, S.; Xing, S.; Mannochio-Russo, H.; Mohanty, I.; Zhao, H. N.; Caraballo-Rodriguez, A. M.; Gomes, P. W. P.; Avalon, N. E.; Northen, T. R.; Bowen, B. P.; Louie, K. B.; Dorrestein, P. C.; Wang, M.; *Nat. Commun.* **2025**, *16*, 4838. [Crossref]
10. Couch, R. D.; Dailey, A.; Zaidi, F.; Navarro, K.; Forsyth, C. B.; Mutlu, E.; Engen, P. A.; Keshavarzian, A.; *PLoS One* **2015**, *10*, e0119362. [Crossref]
11. Yu, H.; Xing, S.; Nierves, L.; Lange, P. F.; Huan, T.; *Anal. Chem.* **2020**, *92*, 7011. [Crossref]
12. Batsoyol, N.; Pullman, B.; Wang, M.; Bandeira, N.; Swanson, S. In *SC22: International Conference for High Performance Computing, Networking, Storage and Analysis*; ACM Digital Library and IEEE Xplore: Dallas, TX, USA, 2022, p. 1-15. [Crossref]
13. Gomes, P. W. P.; Mannochio-Russo, H.; Schmid, R.; Zuffa, S.; Damiani, T.; Quiros-Guerrero, L.-M.; Caraballo-Rodríguez, A. M.; Zhao, H. N.; Yang, H.; Xing, S.; Charron-Lamoureux, V.; Chigumba, D. N.; Sedio, B. E.; Myers, J. A.; Allard, P.-M.; Harwood, T. V.; Tamayo-Castillo, G.; Kang, K. B.; Defossez, E.; Koolen, H. H. F.; da Silva, M. N.; E Silva, C. Y. Y.; Rasmann, S.; Walker, T. W. N.; Glauser, G.; Chaves-Fallas, J. M.; David,

B.; Kim, H.; Lee, K. H.; Kim, M. J.; Choi, W. J.; Keum, Y.-S.; de Lima, E. J. S. P.; de Medeiros, L. S.; Bataglion, G. A.; Costa, E. V.; da Silva, F. M. A.; Carvalho, A. R. V.; Reis, J. D. E.; Pamplona, S.; Jeong, E.; Lee, K.; Kim, G. J.; Kil, Y.-S.; Nam, J.-W.; Choi, H.; Han, Y. K.; Park, S. Y.; Lee, K. Y.; Hu, C.; Dong, Y.; Sang, S.; Morrison, C. R.; Borges, R. M.; Teixeira, A. M.; Lee, S. Y.; Lee, B. S.; Jeong, S. Y.; Kim, K. H.; Rutz, A.; Gaudry, A.; Bruelhart, E.; Kappers, I. F.; Karlova, R.; Meisenburg, M.; Berdaguer, R.; Tello, J. S.; Henderson, D.; Cayola, L.; Wright, S. J.; Allen, D. N.; Anderson-Teixeira, K. J.; Baltzer, J. L.; Lutz, J. A.; McMahon, S. M.; Parker, G. G.; Parker, J. D.; Northen, T. R.; Bowen, B. P.; Pluskal, T.; van der Hooft, J. J. J.; Carver, J. J.; Bandeira, N.; Pullman, B. S.; Wolfender, J.-L.; Kersten, R. D.; Wang, M.; Dorrestein, P. C.; *bioRxiv*, 2024. [Crossref]

14. Zuffa, S.; Schmid, R.; Bauermeister, A.; Gomes, P. W. P.; Caraballo-Rodriguez, A. M.; El Abiead, Y.; Aron, A. T.; Gentry, E. C.; Zemlin, J.; Meehan, M. J.; Avalon, N. E.; Cichewicz, R. H.; Buzun, E.; Terrazas, M. C.; Hsu, C.-Y.; Oles, R.; Ayala, A. V.; Zhao, J.; Chu, H.; Kuijpers, M. C. M.; Jackrel, S. L.; Tugizimana, F.; Nephali, L. P.; Dubery, I. A.; Madala, N. E.; Moreira, E. A.; Costa-Lotufo, L. V.; Lopes, N. P.; Rezende-Teixeira, P.; Jimenez, P. C.; Rimal, B.; Patterson, A. D.; Traxler, M. F.; Pessotti, R. de C.; Alvarado-Villalobos, D.; Tamayo-Castillo, G.; Chaverri, P.; Escudero-Leyva, E.; Quiros-Guerrero, L.-M.; Bory, A. J.; Joubert, J.; Rutz, A.; Wolfender, J.-L.; Allard, P.-M.; Sichert, A.; Pontrelli, S.; Pullman, B. S.; Bandeira, N.; Gerwick, W. H.; Gindro, K.; Massana-Codina, J.; Wagner, B. C.; Forchhammer, K.; Petras, D.; Aiosa, N.; Garg, N.; Liebeke, M.; Bourceau, P.; Kang, K. B.; Gadhavi, H.; de Carvalho, L. P. S.; Silva Dos Santos, M.; Pérez-Lorente, A. I.; Molina-Santiago, C.; Romero, D.; Franke, R.; Brönstrup, M.; Vera Ponce de León, A.; Pope, P. B.; La Rosa, S. L.; La Barbera, G.; Roager, H. M.; Laursen, M. F.; Hammerle, F.; Siewert, B.; Peintner, U.; Licona-Cassani, C.; Rodriguez-Orduña, L.; Rampler, E.; Hildebrand, F.; Koellensperger, G.; Schoeny, H.; Hohenwallner, K.; Panzenboeck, L.; Gregor, R.; O'Neill, E. C.; Roxborough, E. T.; Odoi, J.; Bale, N. J.; Ding, S.; Sinninghe Damsté, J. S.; Guan, X. L.; Cui, J. J.; Ju, K.-S.; Silva, D. B.; Silva, F. M. R.; da Silva, G. F.; Koolen, H. H. F.; Grundmann, C.; Clement, J. A.; Mohimani, H.; Broders, K.; McPhail, K. L.; Ober-Singleton, S. E.; Rath, C. M.; McDonald, D.; Knight, R.; Wang, M.; Dorrestein, P. C.; *Nat. Microbiol.* **2024**, *9*, 336. [Crossref]
15. West, K. A.; Schmid, R.; Gauglitz, J. M.; Wang, M.; Dorrestein, P. C.; *Npj Sci. Food* **2022**, *6*, 22. [Crossref]
16. Zhao, H. N.; Kvitne, K. E.; Brungs, C.; Mohan, S.; Charron-Lamoureux, V.; Bittremieux, W.; Tang, R.; Schmid, R.; Lamichhane, S.; El Abiead, Y.; Andalibi, M. S.; Mannochio-Russo, H.; Ambre, M.; Avalon, N. E.; Bryant, M.; Caraballo-Rodríguez, A. M.; Maya, M. C.; Chin, L.; Ellis, R. J.; Franklin, D.; Girod, S.; Gomes, P. W. P.; Hansen, L.; Heaton, R.; Iudicello, J. E.; Jarmusch, A. K.; Khatib, L.; Letendre, S.; Magyari, S.; McDonald, D.; Mohanty, I.; Cumsille, A.; Moore, D. J.; Rajkumar, P.; Ross, D. H.; Sapre, H.; Shahneh, M. R. Z.; Thomas, S. P.; Tribelhorn, C.; Tubb, H. M.; Walker, C.; Wang, C. X.; Xing, S.; Zemlin, J.; Zuffa, S.; Wishart, D. S.; Kaddurah-Daouk, R.; Wang, M.; Raffatellu, M.; Zengler, K.; Pluskal, T.; Xu, L.; Knight, R.; Tsunoda, S. M.; Dorrestein, P. C.; *bioRxiv*, 2024. [Crossref]
17. Dorrestein, P. C.; *MassIVE MSV000090788*, 2022. [Link] acessed in January 2026
18. Gomes, P. W. P.; Mannochio-Russo, H.; Mao, J.; Zhao, H. N.; Ancira, J.; Tipton, C. D.; Dorrestein, P. C.; Li, M.; *mSystems* **2024**, *9*, e0111923. [Crossref]
19. Schmid, R.; Heuckeroth, S.; Korf, A.; Smirnov, A.; Myers, O.; Dyrlund, T. S.; Bushuiev, R.; Murray, K. J.; Hoffmann, N.; Lu, M.; Sarvepalli, A.; Zhang, Z.; Fleischauer, M.; Dührkop, K.; Wesner, M.; Hoogstra, S. J.; Rudt, E.; Mokshyna, O.; Brungs, C.; Ponomarov, K.; Mutabdžija, L.; Damiani, T.; Pudney, C. J.; Earll, M.; Helmer, P. O.; Fallon, T. R.; Schulze, T.; Rivas-Ubach, A.; Bilbao, A.; Richter, H.; Nothias, L.-F.; Wang, M.; Orešič, M.; Weng, J.-K.; Böcker, S.; Jeibmann, A.; Hayen, H.; Karst, U.; Dorrestein, P. C.; Petras, D.; Du, X.; Pluskal, T.; *Nat. Biotechnol.* **2023**, *41*, 447. [Crossref]
20. Pakkir Shah, A. K.; Walter, A.; Ottosson, F.; Russo, F.; Navarro-Diaz, M.; Boldt, J.; Kalinski, J.-C. J.; Kontou, E. E.; Elofson, J.; Polyzois, A.; González-Marín, C.; Farrell, S.; Aggerbeck, M. R.; Pruksatrakul, T.; Chan, N.; Wang, Y.; Pöchhacker, M.; Brungs, C.; Cámara, B.; Caraballo-Rodríguez, A. M.; Cumsille, A.; de Oliveira, F.; Dührkop, K.; El Abiead, Y.; Geibel, C.; Graves, L. G.; Hansen, M.; Heuckeroth, S.; Knoblauch, S.; Kostenko, A.; Kuijpers, M. C. M.; Mildau, K.; Papadopoulos Lambidis, S.; Gomes, P. W. P.; Schramm, T.; Steuer-Lodd, K.; Stincone, P.; Tayyab, S.; Vitale, G. A.; Wagner, B. C.; Xing, S.; Yazzie, M. T.; Zuffa, S.; de Kruijff, M.; Beemelmanns, C.; Link, H.; Mayer, C.; van der Hooft, J. J. J.; Damiani, T.; Pluskal, T.; Dorrestein, P.; Stanstrup, J.; Schmid, R.; Wang, M.; Aron, A.; Ernst, M.; Petras, D.; *Nat. Protoc.* **2024**, *20*, 92. [Crossref]
21. Wang, M.; Carver, J. J.; Phelan, V. V.; Sanchez, L. M.; Garg, N.; Peng, Y.; Nguyen, D. D.; Watrous, J.; Kapono, C. A.; Luzzatto-Knaan, T.; Porto, C.; Bouslimani, A.; Melnik, A. V.; Meehan, M. J.; Liu, W.-T.; Crüsemann, M.; Boudreau, P. D.; Esquenazi, E.; Sandoval-Calderón, M.; Kersten, R. D.; Pace, L. A.; Quinn, R. A.; Duncan, K. R.; Hsu, C.-C.; Floros, D. J.; Gavilan, R. G.; Kleigrewe, K.; Northen, T.; Dutton, R. J.; Parrot, D.; Carlson, E. E.; Aigle, B.; Michelsen, C. F.; Jelsbak, L.; Sohlenkamp, C.; Pevzner, P.; Edlund, A.; McLean, J.; Piel, J.; Murphy, B. T.; Gerwick, L.; Liaw, C.-C.; Yang, Y.-L.; Humpf, H.-U.; Maansson, M.; Keyzers, R. A.; Sims, A. C.; Johnson, A. R.; Sidebottom, A. M.; Sedio, B. E.; Klitgaard, A.; Larson, C. B.; P, C. A. B.; Torres-Mendoza, D.; Gonzalez, D. J.; Silva, D. B.; Marques, L. M.; Demarque, D. P.; Pociute, E.; O'Neill,

E. C.; Briand, E.; Helfrich, E. J. N.; Granatosky, E. A.; Glukhov, E.; Ryffel, F.; Houson, H.; Mohimani, H.; Kharbush, J. J.; Zeng, Y.; Vorholt, J. A.; Kurita, K. L.; Charusanti, P.; McPhail, K. L.; Nielsen, K. F.; Vuong, L.; Elfeki, M.; Traxler, M. F.; Engene, N.; Koyama, N.; Vining, O. B.; Baric, R.; Silva, R. R.; Mascuch, S. J.; Tomasi, S.; Jenkins, S.; Macherla, V.; Hoffman, T.; Agarwal, V.; Williams, P. G.; Dai, J.; Neupane, R.; Gurr, J.; Rodríguez, A. M. C.; Lamsa, A.; Zhang, C.; Dorrestein, K.; Duggan, B. M.; Almaliti, J.; Allard, P.-M.; Phapale, P.; Nothias, L.-F.; Alexandrov, T.; Litaudon, M.; Wolfender, J.-L.; Kyle, J. E.; Metz, T. O.; Peryea, T.; Nguyen, D.-T.; VanLeer, D.; Shinn, P.; Jadhav, A.; Müller, R.; Waters, K. M.; Shi, W.; Liu, X.; Zhang, L.; Knight, R.; Jensen, P. R.; Palsson, B. O.; Pogliano, K.; Linington, R. G.; Gutiérrez, M.; Lopes, N. P.; Gerwick, W. H.; Moore, B. S.; Dorrestein, P. C.; Bandeira, N.; *Nat. Biotechnol.* **2016**, *34*, 828. [Crossref]

22. Nothias, L.-F.; Petras, D.; Schmid, R.; Dührkop, K.; Rainer, J.; Sarvepalli, A.; Protsyuk, I.; Ernst, M.; Tsugawa, H.; Fleischauer, M.; Aicheler, F.; Aksenov, A. A.; Alka, O.; Allard, P.-M.; Barsch, A.; Cachet, X.; Caraballo-Rodriguez, A. M.; Da Silva, R. R.; Dang, T.; Garg, N.; Gauglitz, J. M.; Gurevich, A.; Isaac, G.; Jarmusch, A. K.; Kameník, Z.; Kang, K. B.; Kessler, N.; Koester, I.; Korf, A.; Le Gouellec, A.; Ludwig, M.; Martin H. C.; McCall, L.-I.; McSayles, J.; Meyer, S. W.; Mohimani, H.; Morsy, M.; Moyne, O.; Neumann, S.; Neuweger, H.; Nguyen, N. H.; Nothias-Esposito, M.; Paolini, J.; Phelan, V. V.; Pluskal, T.; Quinn, R. A.; Rogers, S.; Shrestha, B.; Tripathi, A.; van der Hooft, J. J. J.; Vargas, F.; Weldon, K. C.; Witting, M.; Yang, H.; Zhang, Z.; Zubeil, F.; Kohlbacher, O.; Böcker, S.; Alexandrov, T.; Bandeira, N.; Wang, M.; Dorrestein, P. C.; *Nat. Methods* **2020**, *17*, 905. [Crossref]
23. GNPS2 - Analysis Hub. [Link] accessed in January 2026
24. Shannon, P.; Markiel, A.; Ozier, O.; Baliga, N. S.; Wang, J. T.; Ramage, D.; Amin, N.; Schwikowski, B.; Ideker, T.; *Genome Res.* **2003**, *13*, 2498. [Crossref]
25. Dührkop, K.; Fleischauer, M.; Ludwig, M.; Aksenov, A. A.; Melnik, A. V.; Meusel, M.; Dorrestein, P. C.; Rousu, J.; Böcker, S.; *Nat. Methods* **2019**, *16*, 299. [Crossref]
26. Schmid, R.; Zuffa, S.; Wang, M.; Thomas, S.; *Zenodo*, 2024. [Crossref]
27. Lex, A.; Gehlenborg, N.; Strobelt, H.; Vuillemot, R.; Pfister, H.; *IEEE Trans. Vis. Comput. Graph.* **2014**, *20*, 1983. [Crossref]
28. Sumner, L. W.; Amberg, A.; Barrett, D.; Beale, M. H.; Beger, R.; Daykin, C. A.; Fan, T. W.-M.; Fiehn, O.; Goodacre, R.; Griffin, J. L.; Hankemeier, T.; Hardy, N.; Harnly, J.; Higashi, R.; Kopka, J.; Lane, A. N.; Lindon, J. C.; Marriott, P.; Nicholls, A. W.; Reily, M. D.; Thaden, J. J.; Viant, M. R.; *Metabolomics* **2007**, *3*, 211. [Crossref]
29. Asakawa, D.; *J. Mass Spectrom.* **2024**, *59*, e5100. [Crossref]
30. Lieser, B.; Liebisch, G.; Drobnik, W.; Schmitz, G.; *J. Lipid Res.* **2003**, *44*, 2209. [Crossref]
31. Bittremieux, W.; Avalon, N. E.; Thomas, S. P.; Kakhkhorov, S. A.; Aksenov, A. A.; Gomes, P. W. P.; Aceves, C. M.; Caraballo-Rodríguez, A. M.; Gauglitz, J. M.; Gerwick, W. H.; Huan, T.; Jarmusch, A. K.; Kaddurah-Daouk, R. F.; Kang, K. B.; Kim, H. W.; Kondić, T.; Mannochio-Russo, H.; Meehan, M. J.; Melnik, A. V.; Nothias, L.-F.; O'Donovan, C.; Panitchpakdi, M.; Petras, D.; Schmid, R.; Schymanski, E. L.; van der Hooft, J. J. J.; Weldon, K. C.; Yang, H.; Xing, S.; Zemlin, J.; Wang, M.; Dorrestein, P. C.; *Nat. Commun.* **2023**, *14*, 8488. [Crossref]
32. Hancock, S. E.; Ailuri, R.; Marshall, D. L.; Brown, S. H. J.; Saville, J. T.; Narreddula, V. R.; Boase, N. R.; Poad, B. L. J.; Trevitt, A. J.; Willcox, M. D. P.; Kelso, M. J.; Mitchell, T. W.; Blanksby, S. J.; *J. Lipid Res.* **2018**, *59*, 1510. [Crossref]
33. Zhang, P.; Chan, W.; Ang, I. L.; Wei, R.; Lam, M. M. T.; Lei, K. M. K.; Poon, T. C. W.; *Sci. Rep.* **2019**, *9*, 6453. [Crossref]
34. Schmuth, M.; Eckmann, S.; Moosbrugger-Martinz, V.; Ortner-Tobider, D.; Blunder, S.; Trafoier, T.; Gruber, R.; Elias, P. M.; *J. Invest. Dermatol.* **2024**, *144*, 989. [Crossref]
35. Li, Y.; Li, Y.; Xu, S.; Chen, Y.; Zhou, P.; Hu, T.; Li, H.; Liu, Y.; Xu, Y.; Ren, J.; Qiu, Y.; Lu, C.; *Pharmacol. Res.* **2022**, *185*, 106491. [Crossref]
36. Huh, W. K.; Masuji, Y.; Tada, J.; Arata, J.; Kaniwa, M.; *Am. J. Contact Dermat.* **2001**, *12*, 35. [Crossref]
37. Yuan, C.; Wang, X.-M.; Guichard, A.; Tan, Y.-M.; Qian, C.-Y.; Yang, L.-J.; Humbert, P.; *Clin. Interv. Aging* **2014**, *9*, 1163. [Crossref]
38. Mock, E. D.; Gagestein, B.; van der Stelt, M.; *Prog. Lipid Res.* **2023**, *89*, 101194. [Crossref]
39. Teranishi, Y.; Kuwahara, H.; Ueda, M.; Takemura, T.; Kusumoto, M.; Nakamura, K.; Sakai, J.; Kimura, T.; Furutani, Y.; Kawashima, M.; Imokawa, G.; Nogami-Itoh, M.; *Int. J. Mol. Sci.* **2020**, *21*, 8789. [Crossref]
40. Hachem, J.-P.; Crumrine, D.; Fluhr, J.; Brown, B. E.; Feingold, K. R.; Elias, P. M.; *J. Invest. Dermatol.* **2003**, *121*, 345. [Crossref]
41. Ilves, L.; Ottas, A.; Kaldvee, B.; Abram, K.; Soomets, U.; Zilmer, M.; Jaks, V.; Kingo, K.; *Acta Derm. Venereol.* **2021**, *101*, adv00407. [Crossref]
42. Torres, T.; Ferreira, E. O.; Gonçalo, M.; Mendes-Bastos, P.; Selores, M.; Filipe, P.; *Acta Med. Port.* **2019**, *32*, 606. [Crossref]
43. Alessandrello, C.; Sanfilippo, S.; Minciullo, P. L.; Gangemi, S.; *Int. J. Mol. Sci.* **2024**, *25*, 5020. [Crossref]
44. Elias, P. M.; *Biochim. Biophys. Acta* **2014**, *1841*, 323. [Crossref]
45. Chen, H.; Zhao, Q.; Zhong, Q.; Duan, C.; Krutmann, J.; Wang, J.; Xia, J.; *Phenomics* **2022**, *2*, 363. [Crossref]
46. Bjerre, R. D.; Holm, J. B.; Palleja, A.; Sølberg, J.; Skov, L.; Johansen, J. D.; *BMC Microbiol.* **2021**, *21*, 256. [Crossref]
47. Bhattacharya, N.; Sato, W. J.; Kelly, A.; Ganguli-Indra, G.; Indra, A. K.; *Trends Mol. Med.* **2019**, *25*, 551. [Crossref]
48. Luo, Y.; Hu, J.; Zhou, Z.; Zhang, Y.; Wu, Y.; Sun, J.; *Front. Med.* **2025**, *12*, 1538194. [Crossref]

49. Khan, A. Q.; Agha, M. V.; Sheikhan, K. S. A. M.; Younis, S. M.; Tamimi, M. A.; Alam, M.; Ahmad, A.; Uddin, S.; Buddenkotte, J.; Steinhoff, M.; *Biomed. Pharmacother.* **2022**, *154*, 113601. [Crossref]
50. Che-Wen, Y.; Lin, F.-L.; Chen, K.-H.; Cheng, Y.-P.; Cheng, Y.-C.; Guo, J.-W.; *Biomed. Pharmacother.* **2025**, *191*, 118508. [Crossref]
51. Stefanovic, N.; Irvine, A. D.; Flohr, C.; *Curr. Treat. Options Allergy* **2021**, *8*, 222. [Crossref]
52. Zhang, Y.; Xu, H.; Tang, Y.; Li, Y.; Zheng, F.; *Sci. Rep.* **2024**, *14*, 23435. [Crossref]
53. Agrawal, R.; Woodfolk, J. A.; *Curr. Allergy Asthma Rep.* **2014**, *14*, 433. [Crossref]
54. You, H.; Liang, Y.; *Clin. Rev. Allergy Immunol.* **2025**, *68*, 49. [Crossref]

Submitted: November 28, 2025
Accepted Article online: January 16, 2026
Final version online: February 3, 2026